RESEARCH ARTICLE
PLANETARY SCIENCES

Earth and Planetary Physics
10: 410–416, 2026
doi: 10.26464/epp2026043

Betatron cooling of electrons in the Martian ionosphere

Xu Bai[1,2], ZuZheng Chen[1,2*], HuiShan Fu[1,2*], ZhiZhong Guo[3], WenDing Fu[1,2], TianYu Zhou[1,2], Zhe Wang[1,2], and Jing Wang[4]

[1]School of Space and Earth Sciences, Beihang University, Beijing 102206, China;

[2]Key Laboratory of Space Environment Monitoring and Information Processing, Ministry of Industry and Information Technology, Beijing 100191, China;

[3]Faculty of Information Engineering and Automation, Kunming University of Science and Technology, Kunming 650504, China;

[4]Planetary Environmental and Astrobiological Research Laboratory (PEARL), School of Atmospheric Sciences, Sun Yat-sen University, Zhuhai 519082, China

Key Points:

- We present evidence of an electron perpendicular energy decrease predominantly driven by betatron cooling in the Martian ionosphere.
- This cooling occurred in 10–150 eV electrons with a power-law distribution.
- An adiabatic model was used to quantitatively reproduce this cooling.

Citation: Bai, X., Chen, Z. Z., Fu, H. S., Guo, Z. Z., Fu, W. D., Zhou, T. Y., Wang, Z., and Wang, J. (2026). Betatron cooling of electrons in the Martian ionosphere. *Earth Planet. Phys.*, *10*(3), 410–416. http://doi.org/10.26464/epp2026043

Abstract: Electron dynamics plays a crucial role in the evolution of the Martian ionosphere. However, the adiabatic process, a classical mechanism for modulating electron energy and pitch-angle distributions, has not been reported in this environment. Utilizing data from the Mars Atmosphere and Volatile EvolutioN (MAVEN) spacecraft, we present evidence of a decrease in electron perpendicular energy predominantly driven by betatron cooling in the Martian ionosphere. The phenomenon was identified within closed magnetic field lines at the edge of the crustal magnetic fields, a region characterized by a convoluted magnetic field topology comprising both closed and open lines. The observed cooling of 10–150 eV electrons with a power-law distribution, enhancing the cigar distribution, was quantitatively reproduced by an adiabatic model. Our study may promote the understanding of electron dynamics in the Martian ionosphere.

Keywords: Mars; Betatron cooling; space plasmas; Martian ionosphere; magnetic fields

1. Introduction

The evolution of the Martian ionosphere is influenced by external environments (Withers et al., 2008; González-Galindo et al., 2021; Peter et al., 2024) and magnetic field topologies and associated internal local plasma processes (Nielsen et al., 2007; Andrews et al., 2018; Guo ZZ et al., 2021; Wang J et al., 2023), with the dominant factors differing significantly between the dayside and nightside regions. The dayside ionosphere, containing a well-defined primary layer and a low-altitude secondary layer (Rishbeth and Garriott, 1969; Gurnett et al., 2008; Haider et al., 2011), results primarily from photoionization of atmospheric neutrals owing to solar extreme ultraviolet (EUV) and X-ray radiation (Gurnett et al., 2008; Morgan et al., 2008; Peter et al., 2024), making it subject to variations driven by solar activity (Mendillo et al., 2006; Bougher et al., 2015; Sánchez-Cano et al., 2016). In contrast, the nightside ionosphere is characterized by a more patchy and sporadic structure (Duru et al., 2006; Nielsen et al., 2007), which is predominantly governed by day-to-night plasma transport (Cui J et al., 2015; Girazian et al., 2017) and the impact ionization by precipitating electrons (Brain et al., 2006; Fillingim et al., 2007).

A convoluted magnetic field topology in the Martian ionosphere (DiBraccio et al., 2018), arising from a combination of crustal magnetic fields and draped interplanetary magnetic fields (IMF), governs particle energy and pitch-angle distributions (Cao YT et al., 2024). The closed crustal magnetic fields serve to shield the ionosphere from the solar wind particles (Brain et al., 2006; Lillis et al., 2009; Dong CF et al., 2015), whereas the open ones facilitate particle precipitation into the ionosphere (Zou H et al., 2010; Hara et al., 2018). Concurrently, the draped IMF may channel solar wind particles for interaction with the ionosphere (Fowler et al., 2021; Azari et al., 2023; Wang J et al., 2023). The magnetic fields also mediate a variety of plasma processes in the ionosphere; for instance, magnetic reconnection driven by interactions between magnetic field lines in opposite directions can energize particles and facilitate their escape from the ionosphere (Drake et al., 2005; Imada et al., 2015; Jiang K et al., 2024; Lin RT et al., 2024a, b, 2025; Fu WD et al., 2025; Huang SY et al., 2025), and field-controlled particle distributions can excite plasma waves that subsequently

First author: X. Bai, xubai@buaa.edu.cn
Correspondence to: Z. Z. Chen, chenzzh@buaa.edu.cn
H. S. Fu, huishanf@gmail.com
Received 18 DEC 2025; Accepted 02 MAR 2026.
First Published online 05 APR 2026.

contribute to particle heating (Ergun et al., 2006; Wang J et al., 2023).

In a slowly varying magnetic field, adiabatic processes modulate particle energy and pitch-angle distribution through changes in magnetic field strength and bounce path length (Fu HS et al., 2011, 2013, 2019, 2020a; Chen ZZ et al., 2023). Specifically, betatron acceleration (cooling) occurs in response to magnetic field strengthening (weakening), increasing (decreasing) perpendicular energy and flux near the 90° pitch angle (Fu HS et al., 2011, 2012, 2013, 2020a; Guo ZZ et al., 2021). Likewise, Fermi acceleration (cooling) emerges in response to a shortening (lengthening) bounce path, increasing (decreasing) parallel energy and flux near 0° and 180° (Fu HS et al., 2011, 2013, 2019, 2020a, b). However, the roles of adiabatic processes in particle dynamics have not been investigated in the Martian ionosphere.

In this study, utilizing data from the Mars Atmosphere and Volatile EvolutioN (MAVEN) mission (Jakosky et al., 2015), we present direct evidence of a weakening in electron perpendicular energy and the formation of pronounced cigar pitch-angle distributions arising from betatron cooling. This process was quantitatively reproduced using an adiabatic model as well.

2. Observations

The level-2 calibrated data from MAVEN are used in this study. Specifically, the magnetic fields are measured by MAVEN's Magnetometer (MAG; Connerney et al., 2015), the electron measurements are from the Solar Wind Electron Analyzer (SWEA) instrument (Mitchell et al., 2016), and the ion (H^+, O^+, and O_2^+) measurements are from the SupraThermal And Thermal Ion Composition (STATIC) instrument (McFadden et al., 2015). The magnetic field map is produced by using magnetic field data from MAG during the 2015–2020 interval (Langlais et al., 2019). All the data are shown in Mars Solar Orbital (MSO) coordinates unless specified, which is defined with the *X*-axis pointing from Mars to the Sun, the *Y*-axis pointing opposite the direction of the Martian orbital velocity component perpendicular to the *X*-axis, and the *Z*-axis completing the right-handed system (Trotignon et al., 2006).

The event of interest was observed between 09:18:00 universal time (UT) and 09:21:00 UT on June 4, 2022. An overview of the event is shown in Figures 1a–1f. Specifically, the magnetic field map at an altitude from 332 to 432 km (Figure 1a), the strength and three components of the magnetic field (Figure 1b), the ion mass spectra from STATIC (Figure 1c), the differential energy flux of ions with a mass-to-charge ratio of 12–44 (Figure 1d), pitch-angle distributions of electrons with energy of 10–150 eV (Figure 1e), and electron differential energy flux (Figure 1f) are presented from top to bottom. This magnetic field map was constructed using average measurements of the magnetic field recorded between 2015 and 2020 at altitudes ranging from 332 to 432 km. Figure 1a shows the base-10 logarithm of the average measurements. During this period, MAVEN cruised near the edge (longitude of ~33°W and latitude of ~1°S) of the crustal magnetic fields at an orbital altitude of approximately 383 km (marked by the black arrow in Figure 1a). The detection of heavy ions (O^+ and O_2^+) with energies of several tens of electron volts at such a low altitude (Figures 1c and 1d), combined with a solar zenith angle of ~170° (not shown), provide clear evidence that MAVEN has encountered the Martian nightside ionosphere (Zhang MHG et al., 1990; Gurnett et al., 2008; Benna et al., 2015; Girazian et al., 2017). This region exhibits a mixed magnetic topology composed of both closed and open field lines, as indicated by the pitch-angle distributions of electrons with energies of 10–150 eV (Figure 1e). The closed field lines are evidenced before 09:19:38 UT (marked by the right dashed line) by the counter-streaming (field-aligned and antifield-aligned) electrons, whereas the subsequent detection of only field-aligned electrons indicates a shift to open ones (09:19:40–09:20:10 UT; Brain et al., 2007). Across both closed and open field line regions, the magnetic field strength is dictated by variations in the magnitude of the dominant B_x component (Figure 1b). A decrease in the magnitude of the B_x component during the interval from 09:18:41 to 09:19:38 UT resulted in a corresponding weakening of the magnetic field strength (Figure 1b). This structure exhibits the characteristics of a magnetic hole, where the weakening of the magnetic field is caused by a reduction in its dominant component (Huang SY et al., 2017, 2021; Chen ZZ et al., 2024). This weakening magnetic field in the closed field line region was accompanied by a reduction of both perpendicular flux and the electron differential energy flux for 10–150 eV electrons (Figures 1e and 1f), which was most evident where the field was weakest. This reduction of perpendicular flux led to a more pronounced cigar distribution (Figure 1e). This phenomenon indicates the occurrence of betatron cooling.

To further investigate this betatron cooling process, a comparative analysis of electron phase space density (PSD) at the energy between 10 and 150 eV was conducted across the magnetic field weakening region (09:18:41–09:19:38 UT, marked by the blue bar in Figure 1e) and its adjacent region (09:18:05–09:18:30 UT, marked by the red bar in Figure 1e) within the closed field line region. Figure 2 presents a comparison of the PSD as a function of electron energy between the two regions, including the profiles for the omnidirectional (Figure 2a), perpendicular (Figure 2b), and field-aligned and antifield-aligned (Figure 2c) directions relative to the magnetic field. Here, the perpendicular direction refers to the pitch angles within ±37.5° of 90°, whereas the field-aligned and antifield-aligned directions correspond to the pitch angles of 0°–37.5° and 142.5°–180°, respectively. The unidirectional definition for field-aligned and antifield-aligned directions is necessary because of the boundaries at 0° and 180°, unlike the symmetric perpendicular case. The decrease in the omnidirectional PSD within the magnetic field weakening region arises primarily from a reduction of the perpendicular PSD, with no significant change in the field-aligned or antifield-aligned PSD across the two regions. Both inside and outside the magnetic field weakening region, the perpendicular PSD follows a power-law spectrum with a nearly identical spectral index of $\gamma = -3.21$, demonstrating a uniform scaling of electron energy across different channels—as expected for betatron cooling (Fillingim et al., 2007; Lillis et al., 2009; Fu HS et al., 2011). In both regions, a power-law spectrum can also be observed in the omnidirectional and field-aligned and antifield-aligned directions, obeying spectral indices of $\gamma = -3.18$ and $\gamma = -3.10$, respectively.

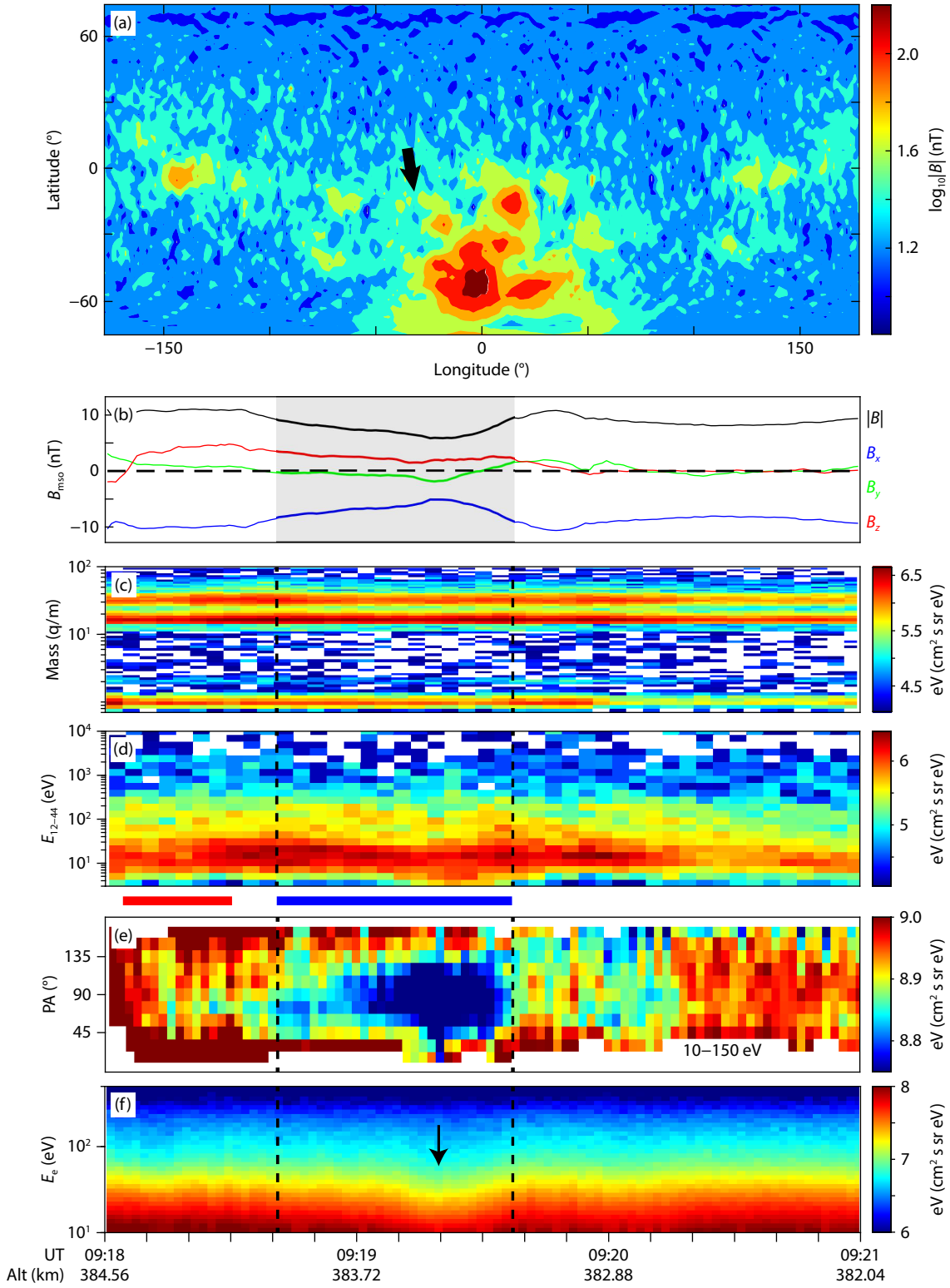

Figure 1. Betatron cooling observed in the Martian ionosphere on June 4, 2022. (a) Magnetic field map at an altitude of 332 to 432 km. The black arrowed line in panel (a) denotes MAVEN's trajectory. (b) Magnetic field B_x, B_y, B_z components and strength ($|B|$); mso, Mars Solar Orbital coordinates. (c) Ion mass spectra from STATIC. (d) Differential energy flux of ions with a mass-to-charge ratio of 12–44. (e) Pitch-angle (PA) distributions of 10–150 eV electrons. (f) Differential energy flux of electrons (E_e). The arrow in panel (f) denotes the region with the weakest magnetic field. The vertical dashed lines mark the magnetic field weakening region. The blue bar in panel (e) denotes the final state of the betatron cooling, whereas the red bar represents its initial state.

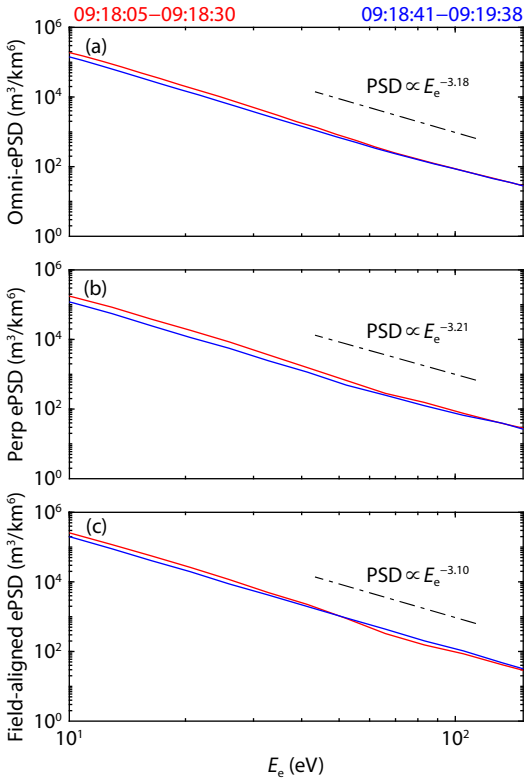

Figure 2. The electron phase space density (ePSD) as a function of electron energy (E_e). (a) The omnidirectional PSD (Omni-ePSD), (b) the perpendicular PSD (Perp ePSD), and (c) the field-aligned and antifield-aligned PSD (Field-aligned ePSD). The blue lines denote the final PSD of the betatron cooling, whereas the red lines represent its initial PSD. The dashed black lines represent the power-law models for fitting electron distributions.

3. Modeling of Betatron Cooling

Adiabatic theory states that the magnetic moment $\mu = \frac{mv_\perp^2}{2B}$ and longitudinal invariant $J = \oint mv_\parallel ds$ are conserved in a slowly varying magnetic field whose change within a particle's gyro-period is negligible. Here, m, $v_\perp$, $v_\parallel$ are the particle's mass, perpendicular velocity, and parallel velocity. Consequently, the particle's perpendicular energy scales with the magnetic field strength ($E_\perp \propto B$), whereas its parallel energy is inversely proportional to the square of the bounce path length ($E_\parallel \propto L^{-2}$). Accordingly, a weakening (strengthening) of the magnetic field strength and a lengthening (shortening) of the bounce path length leads to betatron cooling (acceleration) and Fermi cooling (acceleration), reducing (enhancing) the particle's perpendicular and parallel energy, respectively.

To determine whether the adiabatic condition is satisfied, we compared the spatial scale of this structure with the electrons' gyro-radii, as well as the time for MAVEN to traverse the structure with the electrons' gyro-period. Given that the magnetic structure co-rotates with Mars, and because Mars' rotational speed is smaller by an order of magnitude than MAVEN's orbital speed, the speed of the spacecraft relative to the structure is primarily dictated by its orbital speed. Therefore, the spatial scale is estimated as the product of MAVEN's speed and the traversal time. The spatial scale of this structure ($L_B = V_M \times T_B \sim 189.24$ km) significantly exceeds the gyro-radius ($\rho_e = \sqrt{2m_eE_e}/q_eB \sim 7.147$ km) for 150 eV electrons. Likewise, the MAVEN traversal time ($T_B \sim 57$ s) is much longer than the electrons' gyro-period ($T_e = 2\pi m_e/q_eB \sim 6.182 \times 10^{-3}$ s). This confirms that the adiabatic condition is satisfied. Here, $V_M \sim 3.32$ km/s, $B \sim 5.779$ nT, m_e, q_e, and E_e are MAVEN's speed, the weakest magnetic field magnitude in this structure, electron mass, elementary charge, and electron energy, respectively.

A model has been established to quantitatively reproduce these adiabatic processes (Fu HS et al., 2013), expressed as

$$E_{1\perp} = F_b \cdot E_{0\perp}, \tag{1}$$

$$E_{1\parallel} = F_f \cdot E_{0\parallel}, \tag{2}$$

where $F_b = B_1/B_0$ and $F_f = (L_0/L_1)^2$ are the betatron and Fermi factors, respectively, and the subscripts 0 and 1 refer to the initial state and final state, respectively. According to this adiabatic model along with Liouville's theorem (Fu HS et al., 2011; Birn et al., 2013), the particle distribution in the final state can be derived from that in the initial state by adjusting the betatron and Fermi factors.

Figure 3 presents the modeling results by treating the electron distribution in the magnetic field weakening region as the final state (marked by the blue bar in Figure 1e) and the electron distribution in its adjacent region as the initial state (marked by the red bar in Figure 1e). The solid curves in Figures 3a and 3b denote the observed pitch-angle distributions (PSDs), time-averaged over the periods 09:18:05–09:18:30 UT and 09:18:41–09:19:38 UT, corresponding respectively to the initial (red) and final (blue) states indicated in Figure 1e. The dashed curves in Figure 3b represent the modeling PSD. The modeling distributions agree well with the observed distributions, where a betatron factor of $F_b = 0.82$ and a Fermi factor of $F_f = 1$ were utilized, roughly consistent with the betatron cooling arising from the magnetic field strength decreasing by a factor of 0.7. The discrepancy of 0.12 between these two parameters indicates that the electron cooling is influenced by nonadiabatic processes alongside the dominant adiabatic process.

4. Conclusions

Utilizing data from the MAVEN spacecraft in this study, we have presented observations of an electron perpendicular energy decrease predominantly driven by betatron cooling in the Martian ionosphere. The phenomenon was identified within closed magnetic field lines at the edge of the crustal magnetic fields, a region characterized by a convoluted magnetic field topology comprising both closed and open lines. This cooling process was observed in 10–150 eV electrons that exhibit a power-law spectrum. This process resulted in a more pronounced cigar distribution and was quantitatively reproduced by an adiabatic model. Our study may promote the understanding of electron dynamics in the Martian ionosphere.

Acknowledgments

This work was supported by the National Natural Science Foundation of China (NSFC; Grant Nos. 42241113, 42350710793,

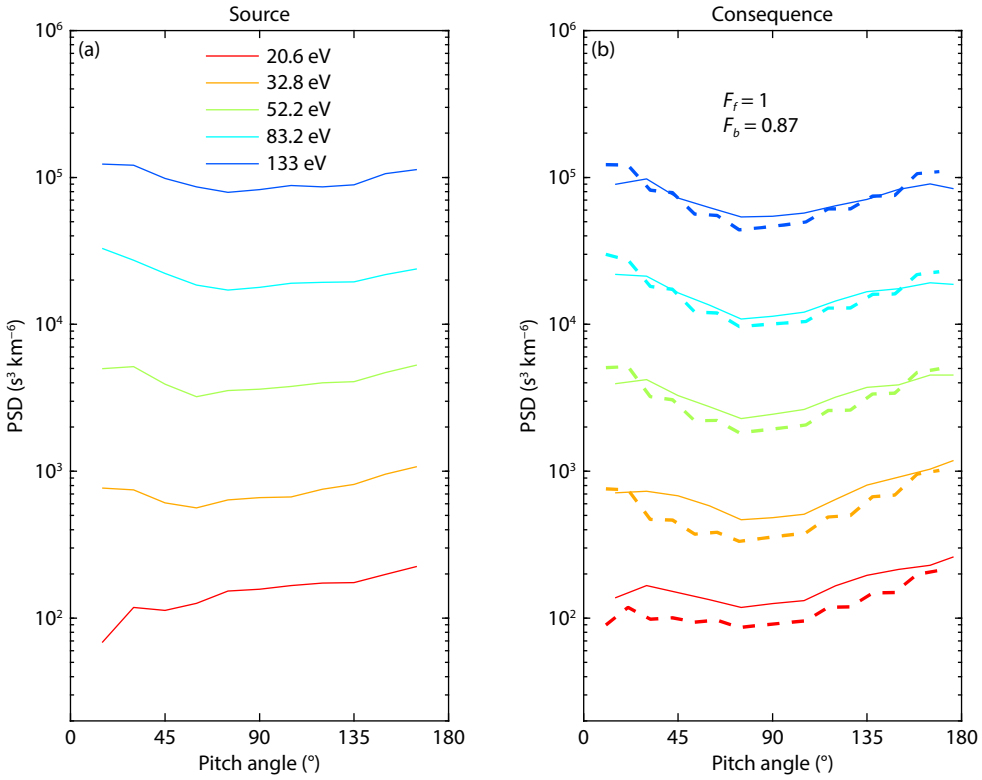

Figure 3. Quantitative analysis of the observed betatron cooling. (a) Phase space density (PSD) versus pitch angles before betatron cooling. (b) PSD versus pitch angles after betatron cooling. The solid curves in panels (a) and (b) denote the observed distributions, whereas the dashed curves in panel (b) represent the modeling distribution.

42304174, 42574225, 424B2032, and 425B2026) and The Fundamental Research Funds for the Central Universities. We express our gratitude to the International Space Science Institute in Beijing (ISSI-BJ) for the travel grant for the team "Understanding Electron-Scale Magnetic Structures in Space Plasmas" led by Elena Grigorenko and HuiShan Fu.

Open Research

All MAVEN data are available on the Planetary Data System website (https://pds-ppi.igpp.ucla.edu).

References

Andrews, D. J., Opgenoorth, H. J., Leyser, T. B., Buchert, S., Edberg, N. J. T., Morgan, D. D., Gurnett, D. A., Kopf, A. J., Fallows, K., and Withers, P. (2018). MARSIS observations of field-aligned irregularities and ducted radio propagation in the Martian ionosphere. *J. Geophys. Res.: Space Phys.*, *123*(8), 6251–6263. https://doi.org/10.1029/2018JA025663

Azari, A. R., Abrahams, E., Sapienza, F., Mitchell, D. L., Biersteker, J., Xu, S., Bowers, C., Pérez, F., DiBraccio, G. A., … Curry, S. (2023). Magnetic field draping in induced magnetospheres: Evidence from the MAVEN mission to Mars. *J. Geophys. Res.: Space Phys.*, *128*(11), e2023JA031546. https://doi.org/10.1029/2023JA031546

Benna, M., Mahaffy, P. R., Grebowsky, J. M., Fox, J. L., Yelle, R. V., and Jakosky, B. M. (2015). First measurements of composition and dynamics of the Martian ionosphere by MAVEN's Neutral Gas and Ion Mass Spectrometer. *Geophys. Res. Lett.*, *42*(21), 8958–8965. https://doi.org/10.1002/2015GL066146

Birn, J., Hesse, M., Nakamura, R., and Zaharia, S. (2013). Particle acceleration in dipolarization events. *J. Geophys. Res.: Space Phys.*, *118*(5), 1960–1971. https://doi.org/10.1002/jgra.50132

Bougher, S. W., Pawlowski, D., Bell, J. M., Nelli, S., McDunn, T., Murphy, J. R., Chizek, M., and Ridley, A. (2015). Mars global ionosphere-thermosphere model: Solar cycle, seasonal, and diurnal variations of the Mars upper atmosphere. *J. Geophys. Res.: Planets*, *120*(2), 311–342. https://doi.org/10.1002/2014JE004715

Brain, D. A., Mitchell, D. L., and Halekas, J. S. (2006). The magnetic field draping direction at Mars from April 1999 through August 2004. *Icarus, 182*(2), 464–473. https://doi.org/10.1016/j.icarus.2005.09.023

Brain, D. A., Lillis, R. J., Mitchell, D. L., Halekas, J. S., and Lin, R. P. (2007). Electron pitch angle distributions as indicators of magnetic field topology near Mars. *J. Geophys. Res.: Space Phys.*, *112*(A9), A09201. https://doi.org/10.1029/2007JA012435

Cao, Y. T., Cui, J., Wu, X. S., Liang, W. J., Fu, R. Q., and Lu, H. Y. (2024). The anisotropy of suprathermal electrons in the Martian ionosphere. *Earth Planet. Phys.*, *8*(3), 459–471. https://doi.org/10.26464/epp2024028

Chen, Z. Z., Liu, C. M., Yu, J., Wang, T. Y., Wang, J., Cui, J., and Cao, J. B. (2023). Electron-scale front of magnetic pile-up region in reconnection exhaust. *J. Geophys. Res.: Space Phys.*, *128*(2), e2022JA030818. https://doi.org/10.1029/2022JA030818

Chen, Z. Z., Wang, T. Y., Liu, Y. Y., Yu, J., Wang, J., Ye, Y. D., Jiang, Y. C., Fu, H. S., Cui, J., … Ergun, R. E. (2024). The electric field and its impact on the pitch angle of trapped electrons in a sub-ion-scale magnetic hole. *Astrophys. J.*, *976*(1), 12. https://doi.org/10.3847/1538-4357/ad7c46

Connerney, J. E. P., Espley, J., Lawton, P., Murphy, S., Odom, J., Oliversen, R., and Sheppard, D. (2015). The MAVEN magnetic field investigation. *Space Sci. Rev.*, *195*(1–4), 257–291. https://doi.org/10.1007/s11214-015-0169-4

Cui, J., Galand, M., Yelle, R. V., Wei, Y., and Zhang, S. J. (2015). Day-to-night transport in the Martian ionosphere: Implications from total electron content measurements. *J. Geophys. Res.: Space Phys.*, *120*(3), 2333–2346. https://doi.org/10.1002/2014JA020788

DiBraccio, G. A., Xu, S., Mitchell, D. L., et al. (2018). The twisted configuration of the Martian magnetotail: MAVEN observations. *Geophys. Res. Lett.*, *45*(10), 4559–4568. https://doi.org/10.1029/2018GL077251

Dong, C. F., Bougher, S. W., Ma, Y. J., Toth, G., Lee, Y., Nagy, A. F., Tenishev, V., Pawlowski, D. J., Combi, M. R., and Najib, D. (2015). Solar wind interaction with the Martian upper atmosphere: Crustal field orientation, solar cycle, and seasonal variations. *J. Geophys. Res.: Space Phys.*, *120*(9), 7857–7872. https://doi.org/10.1002/2015JA020990

Drake, J. F., Shay, M. A., Thongthai, W., and Swisdak, M. (2005). Production of energetic electrons during magnetic reconnection. *Phys. Rev. Lett.*, *94*(9), 095001. https://doi.org/10.1103/PhysRevLett.94.095001

Duru, F., Gurnett, D. A., Averkamp, T. F., Kirchner, D. L., Huff, R. L., Persoon, A. M., Plaut, J. J., and Picardi, G. (2006). Magnetically controlled structures in the ionosphere of Mars. *J. Geophys. Res.: Space Physics*, *111*(A12), A12204. https://doi.org/10.1029/2006JA011975

Ergun, R. E., Andersson, L., Peterson, W. K., Brain, D., Delory, G. T., Mitchell, D. L., Lin, R. P., and Yau, A. W. (2006). Role of plasma waves in Mars' atmospheric loss. *Geophys. Res. Lett.*, *33*(14), L14103. https://doi.org/10.1029/2006GL025785

Fillingim, M. O., Peticolas, L. M., Lillis, R. J., Brain, D. A., Halekas, J. S., Mitchell, D. L., Lin, R. P., Lummerzheim, D., Bougher, S. W., and Kirchner, D. L. (2007). Model calculations of electron precipitation induced ionization patches on the nightside of Mars. *Geophys. Res. Lett.*, *34*(12), L12101. https://doi.org/10.1029/2007GL029986

Fowler, C. M., Hanley, K. G., McFadden, J. P., Chaston, C. C., Bonnell, J. W., Halekas, J. S., Espley, J. R., DiBraccio, G. A., Schwartz, S. J., … Lillis, R. J. (2021). MAVEN observations of low frequency steepened magnetosonic waves and associated heating of the Martian nightside ionosphere. *J. Geophys. Res.: Space Phys.*, *126*(10), e2021JA029615. https://doi.org/10.1029/2021JA029615

Fu, H. S., Khotyaintsev, Y. V., André, M., and Vaivads, A. (2011). Fermi and betatron acceleration of suprathermal electrons behind dipolarization fronts. *Geophys. Res. Lett.*, *38*(16), L16104. https://doi.org/10.1029/2011GL048528

Fu, H. S., Khotyaintsev, Y. V., Vaivads, A., André, M., Sergeev, V. A., Huang, S. Y., Kronberg, E. A., and Daly, P. W. (2012). Pitch angle distribution of suprathermal electrons behind dipolarization fronts: A statistical overview. *J. Geophys. Res.: Space Phys.*, *117*(A12), A12221. https://doi.org/10.1029/2012JA018141

Fu, H. S., Khotyaintsev, Y. V., Vaivads, A., Retinò, A., and André, M. (2013). Energetic electron acceleration by unsteady magnetic reconnection. *Nat. Phys.*, *9*(7), 426–430. https://doi.org/10.1038/nphys2664

Fu, H. S., Xu, Y., Vaivads, A., and Khotyaintsev, Y. V. (2019). Super-efficient electron acceleration by an isolated magnetic reconnection. *Astrophys. J. Lett.*, *870*(2), L22. https://doi.org/10.3847/2041-8213/aafa75

Fu, H. S., Grigorenko, E. E., Gabrielse, C., Liu, C. M., Lu, S., Hwang, K. J., Zhou, X. Z., Wang, Z., and Chen, F. (2020a). Magnetotail dipolarization fronts and particle acceleration: A review. *Sci. China Earth Sci.*, *63*(2), 235–256. https://doi.org/10.1007/s11430-019-9551-y

Fu, H. S., Zhao, M. J., Yu, Y., and Wang, Z. (2020b). A new theory for energetic electron generation behind dipolarization front. *Geophys. Res. Lett.*, *47*(6), e2019GL086790. https://doi.org/10.1029/2019GL086790

Fu, W. D., Fu, H. S., Zhang, W. Z., Yu, Y., and Cao, J. B. (2025). Compression of Earth's magnetopause down to 5 R_E during the superstorm on 10 May 2024. *Geophys. Res. Lett.*, *52*(5), e2024GL114040. https://doi.org/10.1029/2024GL114040

Girazian, Z., Mahaffy, P., Lillis, R. J., Benna, M., Elrod, M., Fowler, C. M., and Mitchell, D. L. (2017). Ion densities in the nightside ionosphere of Mars: Effects of electron impact ionization. *Geophys. Res. Lett.*, *44*(22), 11248–11256. https://doi.org/10.1002/2017GL075431

González-Galindo, F., Peter, K., Pätzold, M., Tellmann, S., Witasse, O., Cardnell, S., and Häusler, B. (2021). Seasonal and geographical variability of the Martian ionosphere from Mars Express observations. *J. Geophys. Res.: Planets*, *126*(2), e2020JE006661. https://doi.org/10.1029/2020JE006661

Guo, Z. Z., Fu, H. S., Cao, J. B., Fan, K., Yao, Z. H., Liu, Y. Y., Chen, Z. Z., Wang, Z., Liu, X. Y., ... Mitchell, D. L. (2021). Betatron cooling of electrons in Martian magnetotail. *Geophys. Res. Lett.*, *48*(13), e2021GL093826. https://doi.org/10.1029/2021GL093826

Gurnett, D. A., Huff, R. L., Morgan, D. D., Persoon, A. M., Averkamp, T. F., Kirchner, D. L., Duru, F., Akalin, F., Kopf, A. J., … Picardi, G. (2008). An overview of radar soundings of the Martian ionosphere from the Mars Express spacecraft. *Adv. Space Res.*, *41*(9), 1335–1346. https://doi.org/10.1016/j.asr.2007.01.062

Haider, S. A., Mahajan, K. K., and Kallio, E. (2011). Mars ionosphere: A review of experimental results and modeling studies. *Rev. Geophys.*, *49*(4), RG4001. https://doi.org/10.1029/2011RG000357

Hara, T., Luhmann, J. G., Leblanc, F., Curry, S. M., Halekas, J. S., Seki, K., Brain, D. A., Harada, Y., McFadden, J. P., … Jakosky, B. M. (2018). Evidence for crustal magnetic field control of ions precipitating into the upper atmosphere of Mars. *J. Geophys. Res.: Space Phys.*, *123*(10), 8572–8586. https://doi.org/10.1029/2017JA024798

Huang, S. Y., Du, J. W., Sahraoui, F., Yuan, Z. G., He, J. S., Zhao, J. S., Le Contel, O., Breuillard, H., Wang, D. D., … Burch, J. L. (2017). A statistical study of kinetic-size magnetic holes in turbulent magnetosheath: MMS observations. *J. Geophys. Res.: Space Phys.*, *122*(8), 8577–8588. https://doi.org/10.1002/2017JA024415

Huang, S. Y., Lin, R. T., Yuan, Z. G., Jiang, K., Wei, Y. Y., Xu, S. B., Zhang, J., Zhang, Z. H., Xiong, Q. Y., and Yu, L. (2021). In situ detection of kinetic-size magnetic holes in the Martian magnetosheath. *Astrophys. J.*, *922*(2), 107. https://doi.org/10.3847/1538-4357/ac2737

Huang, S. Y., Xiong, Q. Y., Jiang, K., Yuan, Z. G., Lin, R. T., and Tang, Y. T. (2025). Recent advances on kinetic simulations and observations of electron diffusion region during magnetic reconnection in space plasmas. *Rev. Mod. Plasma Phys.*, *9*(1), 4. https://doi.org/10.1007/s41614-025-00179-6

Imada, S., Hirai, M., and Hoshino, M. (2015). Energetic ion acceleration during magnetic reconnection in the Earth's magnetotail. *Earth Planets Space*, *67*, 203. https://doi.org/10.1186/s40623-015-0372-2

Jakosky, B. M., Lin, R. P., Grebowsky, J. M., Luhmann, J. G., Mitchell, D. F., Beutelschies, G., Priser, T., Acuna, M., Andersson, L., … Zurek, R. (2015). The *Mars Atmosphere and Volatile Evolution (MAVEN)* mission. *Space Sci. Rev.*, *195*(1–4), 3–48. https://doi.org/10.1007/s11214-015-0139-x

Jiang, K., Huang, S. Y., Yuan, Z. G., Xiong, Q. Y., Xu, S. B., and Lin, R. T. (2024). Observations of energy conversion caused by magnetic reconnection at a dipolarization front. *Geophys. Res. Lett.*, *51*(6), e2023GL107919. https://doi.org/10.1029/2023GL107919

Langlais, B., Thébault, E., Houliez, A., Purucker, M. E., and Lillis, R. J. (2019). A new model of the crustal magnetic field of Mars using MGS and MAVEN. *J. Geophys. Res.: Planets*, *124*(6), 1543–1569. https://doi.org/10.1029/2018JE005854

Lillis, R. J., Fillingim, M. O., Peticolas, L. M., Brain, D. A., Lin, R. P., and Bougher, S. W. (2009). Nightside ionosphere of Mars: Modeling the effects of crustal magnetic fields and electron pitch angle distributions on electron impact ionization. *J. Geophys. Res.: Planets*, *114*(E11), E11009. https://doi.org/10.1029/2009JE003379

Lin, R. T., Huang, S. Y., Yuan, Z. G., Jiang, K., Xu, S. B., Wei, Y. Y., Xiong, Q. Y., Zhang, J., Wang, Z., and Yu, L. (2024a). Observation of interchange reconnection on Mars. *Astrophys. J.*, *960*(1), 68. https://doi.org/10.3847/1538-4357/ad0e62

Lin, R. T., Huang, S. Y., Yuan, Z. G., Jiang, K., Wu, H. H., and Xiong, Q. Y. (2024b). Direct observations of magnetic reconnections at the magnetopause of the Martian mini-magnetosphere. *Geophys. Res. Lett.*, *51*(13), e2024GL108880. https://doi.org/10.1029/2024GL108880

Lin, R. T., Huang, S. Y., Wang, Y. M., Xiong, Q. Y., Yuan, Z. G., Wu, H. H., Jiang, K., Wang, G. Q., Chi, Y. T., and Zhang, T. L. (2025). Direct observations of acceleration of planetary ions from Mars' ionosphere through magnetic reconnection when IMF rotates. *Geophys. Res. Lett.*, *52*(22), e2025GL118290. https://doi.org/10.1029/2025GL118290

McFadden, J. P., Kortmann, O., Curtis, D., Dalton, G., Johnson, G., Abiad, R., Sterling, R., Hatch, K., Berg, P., … Jakosky, B. (2015). MAVEN SupraThermal and Thermal Ion Composition (STATIC) instrument. *Space Sci. Rev.*, *195*(1), 199–256. https://doi.org/10.1007/s11214-015-0175-6

Mendillo, M., Withers, P., Hinson, D., Rishbeth, H., and Reinisch, B. (2006). Effects of solar flares on the ionosphere of Mars. *Science*, *311*(5764), 1135–1138. https://doi.org/10.1126/science.1122099

Mitchell, D. L., Mazelle, C., Sauvaud, J. A., Thocaven, J. J., Rouzaud, J., Fedorov,

A., Rouger, P., Toublanc, D., Taylor, E., … Jakosky, B. M. (2016). The MAVEN solar wind electron analyzer. *Space Sci. Rev.*, *200*(1), 495–528. https://doi.org/10.1007/s11214-015-0232-1

Morgan, D. D., Gurnett, D. A., Kirchner, D. L., Fox, J. L., Nielsen, E., and Plaut, J. J. (2008). Variation of the Martian ionospheric electron density from Mars Express radar soundings. *J. Geophys. Res.: Space Phys.*, *113*(A9), A09303. https://doi.org/10.1029/2008JA013313

Nielsen, E., Fraenz, M., Zou, H., Wang, J. S., Gurnett, D. A., Kirchner, D. L., Morgan, D. D., Huff, R., Safaeinili, A., … Lundin, R. (2007). Local plasma processes and enhanced electron densities in the lower ionosphere in magnetic cusp regions on Mars. *Planet. Space Sci.*, *55*(14), 2164–2172. https://doi.org/10.1016/j.pss.2007.07.003

Peter, K., Sánchez-Cano, B., Němec, F., González-Galindo, F., Kopf, A. J., Lester, M., Pätzold, M., Regan, C. E., and Holmström, M. (2024). The ionosphere of Mars after 20 years of Mars Express contributions. *Space Sci. Rev.*, *220*(5), 41. https://doi.org/10.1007/s11214-024-01078-x

Rishbeth, H., and Garriott, O. K. (1969). *Introduction to Ionospheric Physics*. New York: Academic Press.

Sánchez-Cano, B., Lester, M., Witasse, O., Milan, S. E., Hall, B. E. S., Cartacci, M., Peter, K., Morgan, D. D., Blelly, P. L., … Pätzold, M. (2016). Solar cycle variations in the ionosphere of Mars as seen by multiple Mars Express data sets. *J. Geophys. Res.: Space Phys.*, *121*(3), 2547–2568. https://doi.org/10.1002/2015JA022281

Trotignon, J. G., Mazelle, C., Bertucci, C., and Acuña, M. H. (2006). Martian shock and magnetic pile-up boundary positions and shapes determined from the Phobos 2 and Mars Global Surveyor data sets. *Planet. Space Sci.*, *54*(4), 357–369. https://doi.org/10.1016/j.pss.2006.01.003

Wang, J., Yu, J., Chen, Z. Z., Xu, X. J., Cui, J., and Cao, J. B. (2023). Local generation of magnetosonic waves by ring beam hot protons in the Martian ionosphere. *Geophys. Res. Lett.*, *50*(9), e2023GL102911. https://doi.org/10.1029/2023GL102911

Withers, P., Mendillo, M., Hinson, D. P., and Cahoy, K. (2008). Physical characteristics and occurrence rates of meteoric plasma layers detected in the Martian ionosphere by the Mars Global Surveyor Radio Science Experiment. *J. Geophys. Res.: Space Phys.*, *113*(A12), A12314. https://doi.org/10.1029/2008JA013636

Zhang, M. H. G., Luhmann, J. G., and Kliore, A. J. (1990). An observational study of the nightside ionospheres of Mars and Venus with radio occultation methods. *J. Geophys. Res.: Space Phys.*, *95*(A10), 17095–17102. https://doi.org/10.1029/JA095iA10p17095

Zou, H., Chen, H. F., Yu, N., Shi, W. H., Yu, X. Q., Zou, J. Q., and Zhong, W. Y. (2010). Effects of Martian crustal magnetic field on its ionosphere. *Sci. China Technol. Sci.*, *53*(6), 1717–1724. https://doi.org/10.1007/s11431-010-3118-1